Measurement of nonlinear coefficient of optical fiber based on small chirped soliton transmission

Shanliang Liu (刘山亮) and Hongjun Zheng (郑宏军)

Institution of Optical Communication, Liaocheng University, Liaocheng 252059

Received September 3, 2007

We measure the waveform and phase curves of short optical pulses before and after transmission over different lengths of fibers by use of the pulse analyzer with the frequency-resolved optical gating (FROG), and numerically simulate pulse evolution under the experimental conditions. The nonlinear coefficient of the fiber is given by comparing the experimental results with the numerical ones. Difference between the experiment and numerical simulation is analyzed.

OCIS codes: 060.0060, 060.5530, 060.2300, 060.4370, 060.2330.
doi: 10.3788/COL20080607.0533.

As transmission data of wave division multiplexing (WDM) or soliton systems increase, the effects of fiber nonlinearity play a decisive role in the design and performance of modern optical communication links. Self-phase modulation (SPM), modulation instability (MI), cross-phase modulation (XPM), and four-wave mixing (FWM) were used for the measurement of nonlinear coefficient[1−4]. The optical soliton results from the balance between the group-velocity dispersion (GVD) and nonlinearity of fibers. Soliton transmission measurement should be a good method for getting the nonlinear coefficient of a fiber. Many soliton transmission experiments were performed[5−11], but no one was used to measure the nonlinear coefficient of the fiber. Recently, we measure the waveform and phase curves of short optical pulses before and after transmission over different lengths of fibers by use of the pulse analyzer with the frequency-resolved optical gating (FROG), and numerically simulate pulse evolution. The nonlinear coefficient of the fiber is given by comparing the experimental and the numerical results. Difference between the experiment and numerical simulation is analyzed.

Figure 1 shows the experimental setup. The tunable semiconductor mode-locked pulse laser TMLL1550 outputs a optical pulse stream with repetition rate $F = 10$ GHz. The pulses go through optical isolator (ISO) and are input into the Er-doped fiber amplifier (EDFA) whose output power ranges from 10 to 30 dBm by changing the electric current of its pump lasers, and is calibrated by a power meter. The output pulses of the EDFA propagates in a segment of standard single-mode fiber, goes through a polarization controller (PC), and then into the pulse analyzer HR200, which gives the frequency spectra, the waveform and the phase curve, the temporal and the spectral full-width at half-maximum[11,12].

The output pulses of the EDFA are measured by the pulse analyzer before the insertion of the fiber at different output powers. The results show that the central wavelength λ of pulse is 1550 nm, the pulses vary with output power in waveform, temporal width, and frequency chirp. The temporal full-width at half-maximum (FWHM) T_{FWHM} decreases from 1.8 to 1.54 ps and the frequency chirp increases from −0.45 to −0.3 as the output power of EDFA increases from 288 to 462 mW. Figure 2 shows the normalized waveform and the phase curves of the pulses at the output power $P_{\mathrm{av}} = 462$ mW. In Fig. 2(a), the measured waveform (solid curve) fits hyperbolic-secant curve (dash-dotted curve) with $T_{\mathrm{FWHM}} = 1.54$ ps. In Fig. 2(b), the normalized time $\tau = T/T_0$ where $T_0 = T_{\mathrm{FWHM}}/1.763 = 0.87$ ps, the solid curve is the measured results and fits the dotted curves which are

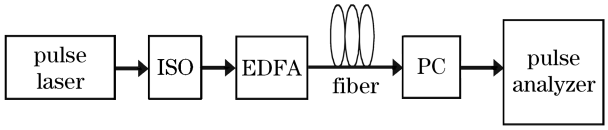

Fig. 1. Experimental setup.

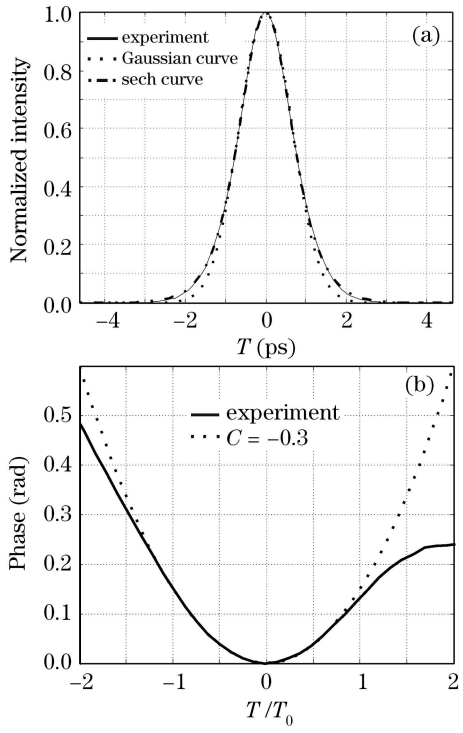

Fig. 2. (a) Waveform curve and (b) phase curve of input pulse at 462 mW.

plotted by phase $\Phi = -C(T/T_0)^2/2$ where $C = -0.3$ is the frequency chirp parameter. It follows that the hyperbolic-secant pulses with $P_0 = P_{\rm av}/(2T_0F) = 26.5$ W, $T_{\rm FWHM} = 1.54$ ps, and $C = -0.3$ go out from the EDFA when $P_{\rm av} = 462$ mW and $\lambda = 1550$ nm.

A segment of standard single-mode fiber is inserted between the EDFA and the PC by the fusion, and the connection loss can be ignored. The GVD parameter of the fiber $\beta_2 = -19.2$ ps^2/km, the attenuation constant $\alpha = 0.188$ dB/km $= 0.0433$ km^{-1}, and the mode-field diameter $w = 10.4$ μm at $\lambda = 1550$ nm. Figure 3 shows the measured waveform curves of output pulses after the transmission over different lengths of fibers. It can be seen that the measured pulse waveforms (solid curves) after the transmission over different lengths of fibers fit well hyperbolic-secant curve (dotted-dash curves). The measured temporal width $T_{\rm FWHM} = 1.82$, 1.59, and 1.75 ps after the transmission over 210-m, 368-m, and 1030-m fiber.

Evolution of an optical pulse in a single-mode fiber is numerically simulated by

$$i\frac{\partial u}{\partial \xi} + \frac{1}{2}\frac{\partial^2 u}{\partial \tau^2} + |u|^2 u = -i\frac{\Gamma}{2}u, \tag{1}$$

under the experimental conditions for initial pulses of the form

$$u(\xi,\tau) = u_0 \,\mathrm{sec\,h}(T/T_0)\exp(-iCT^2/T_0^2), \tag{2}$$

where $T_0 = 0.87$ ps, $C = -0.3$, $u_0 = (P_0/P_1)^{1/2}$, $P_0 = 26.5$ W, $P_1 = 1/(\gamma L_{\rm D})$ is the peak power of fundamental soliton without frequency chirp, $L_{\rm D} = T_0^2/|\beta_2| = 39.7$ m is the dispersion length; $\xi = z/L_{\rm D}$, τ, $\Gamma = \alpha L_{\rm D}$ are the normalized propagation distance, time, and fiber loss, respectively, and the nonlinear coefficient of the fiber is

$$\gamma = \frac{8n_2}{\lambda w^2}, \tag{3}$$

where $n_2 = \chi^{(3)}_{xxxx}/(8n)$ is nonlinear refractive-index coefficient of fiber, $\chi^{(3)}_{xxxx}$ is the third-order nonlinear susceptibility tensor, n is linear refractive index. If $\Gamma = 0$, Eq. (1) becomes the nonlinear Schrödinger equation which has the fundamental soliton solution $u(\xi,\tau) = \mathrm{sec\,h}(\tau)$. Figure 4 shows the pulse waveform curves obtained by the numerical simulation when $u_0 = 1$ after propagating over the different lengths of fibers. It is found that the pulse waveform varies with propagation distance, which is different from the experiments. The simulated waveform curve (dashed curve) obviously deviates from hyperbolic-secant curve (dashed-dotted curve) on bottom after propagating over the 210-m fiber (about $5.3L_{\rm D}$) as shown in Fig. 4(a).

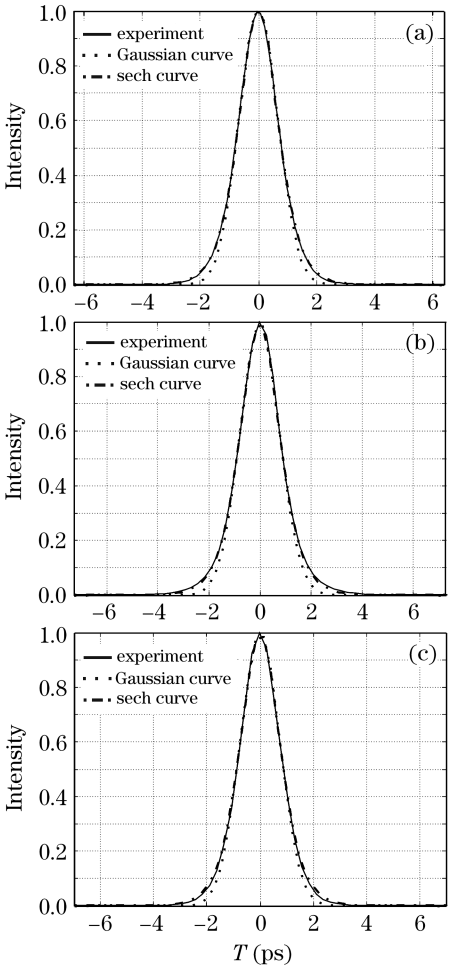

Fig. 3. Measured waveform curves of output pulses after the transmission over the (a) 210-m fiber, (b) 368-m fiber, and (c) 1030-m fiber.

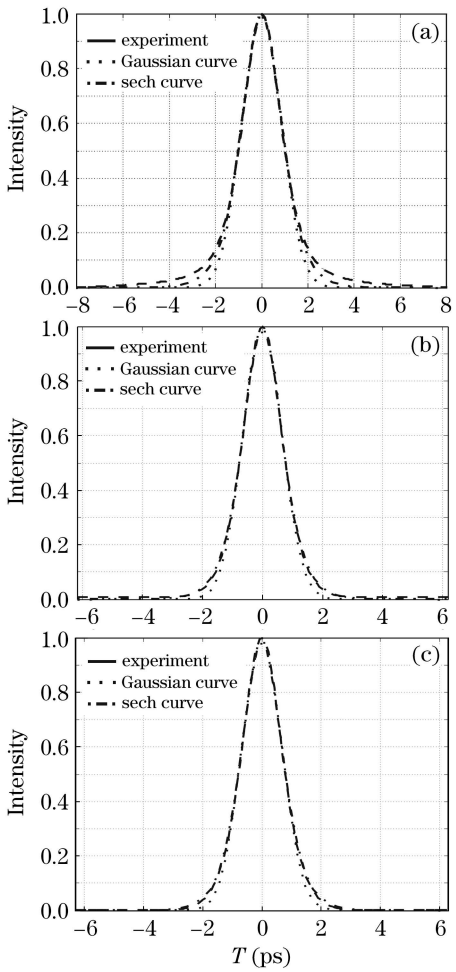

Fig. 4. Simulated waveform of output pulses after propagating over the (a) 210-m fiber, (b) 368-m fiber, and (c) 1030-m fiber.

The intensity decreases on the edges much slower than the hyperbolic-secant curve. We numerically simulate the pulse evolution under the experimental conditions by use of the higher-order nonlinear Schrödinger equation including the higher-order effects such as third-order dispersion, self-steeping, and self-frequency shift. The numerical results including the higher-order effects are almost the same as the above. There are two possible reasons on the difference between the theory and experiment. One is that the waveform and phase curves of input pulse are not exactly described by Eq. (2). The other is that nonlinear refractive index can be expressed as n_2P only for continuous-wave (CW) with power density P. It is further to be examined experimentally whether the expression is valid for such an optical pulse. The lowest-order nonlinear effects originate from the third-order nonlinear susceptibility $\chi^{(3)}$, which is responsible for phenomena such as third-order harmonic generation, FWM, and nonlinear refraction or self-focusing of light beam. Theoretically, the expression n_2P and $|u|^2u$ in Eq. (1) are valid for an optical pulse only when other effects can be ignored and $\chi^{(3)}_{xxxx}(\omega_1,\omega_2,\omega_3.\omega_4) = \chi^{(3)}_{xxxx}(\omega_1,\omega_2) = \chi^{(3)}_{xxxx}(\omega) = 8nn_2$, where $\chi^{(3)}_{xxxx}(\omega)$ and $\chi^{(3)}_{xxxx}(\omega_1,\omega_2)$ are, respectively, responsible for self-focusing or nonlinear phase shift of CW induced by itself and by another CW with different frequencies, and $\chi^{(3)}_{xxxx}(\omega_1,\omega_2,\omega_3.\omega_4)$ for FWM. The simulated intensity is slight stronger than the hyperbolic-secant curve only on the outer edges ($|T| > 3$ ps) after the transmission over 368-m (about $9.3L_{\rm D}$) as shown in Fig. 4(b) and fits well hyperbolic-secant curve after the transmission over 1030-m (about $25.9L_{\rm D}$) as shown in Fig. 4(c).

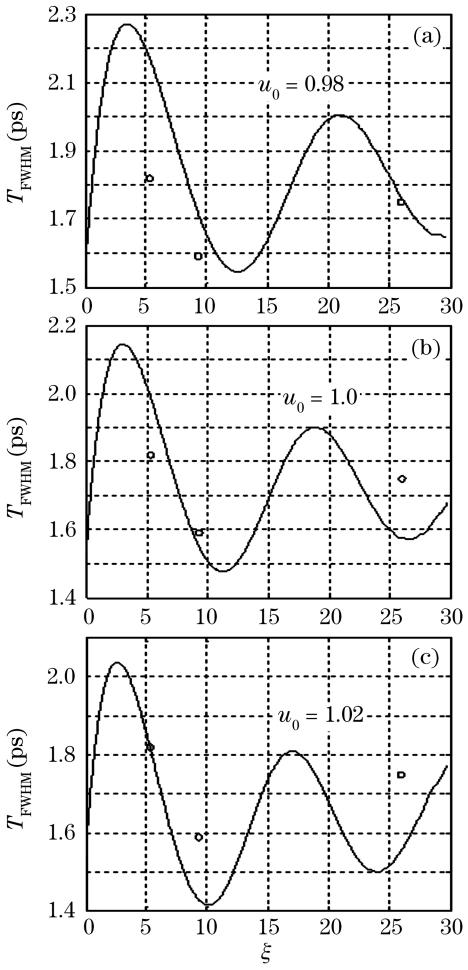

Fig. 5. Variation of temporal FWHM of output pulses with the normalized propagation distance ξ.

Figure 5 shows variation of the pulse width with the normalized propagation distance when $u_0 = 0.98$, 1.0 and 1.02, respectively. The solid curve is the simulated result, and the circles are the measured temporal FWHM after the transmission over 210-m, 368-m, and 1030-m fibers, respectively. It is found that the temporal width of output pulse oscillates with propagation, the variation of pulse width is very sensitive to u_0 and fits well the experimental results when $u_0 = 1.0$, namely, $P_1 = P_0$. It follows that the nonlinear coefficient $\gamma = 1/(P_1L_{\rm D}) = 0.95$ $\rm W^{-1}{\cdot}km^{-1}$. The nonlinear refractive-index coefficient $n_2 = 2\times10^{-20}$ $\rm m^2/W$ is obtained from Eq. (3), which is slight smaller than the previous measured values[1−4]. The small difference can be attributed to dependence of the nonlinear refractive index on pulse width[4].

In summary, output pulses of EDFA vary with its output power in waveform and chirp. The hyperbolic secant pulses with small chirp at 462 mW after propagating over different lengths of standard single-mode fibers are experimentally measured and numerically simulated. The measured results fit well the numerical simulation when the input power is equal to fundamental soliton power, and the nonlinear coefficent of 0.95 $\rm W^{-1}{\cdot}km^{-1}$ is obtained.

This work was supported by the National Natural Science Foundation of China (No. 60778017), the Science and Technology Key Project of Shandong Education Department (No. J05C09), and the Key Laboratory of Optical Communication Technology. S. Liu's e-mail address is shanliangliu@yahoo.com.cn.

References

1. T. Kato, Y. Suetsugu, M. Takagi, E. Sasaoka, and M. Nishimura, Opt. Lett. **20,** 988 (1995).
2. A. Boskovic, S. V. Chernikov, J. R. Taylor, L. Gruner-Nielsen, and O. A. Levring, Opt. Lett. **21,** 1966 (1996).
3. G. P. Agarawal, *Nonlinear Fiber Optics* (3rd edn.) (Elsevier (Singapore) Pte Ltd., 2005) pp. 447 – 453.
4. S. K. Kim, H. S. Moon, and J. -C. Seo, Opt. Lett. **30,** 1120 (2005).
5. L. F. Mollenauer, R. H. Stolen, and J. P. Gordon, Phys. Rev. Lett. **45,** 1095 (1980).
6. J. J .Yu, B. J. Yang, K. J. Guan, X. Zhang, and Q. Yang, Acta Opt. Sin. (in Chinese) **18,** 446 (1998).
7. J. Wu, C. Y. Lou, Y. H. Li, and Y. Z. Gao, Acta Phys. Sin. (in Chinese) **47,** 519 (1998).
8. Z. M. Huang, F. Wu, Z. M. Jiang, W. Zhang, A. Xu, and Q. Xiang, Acta Photon. Sin. (in Chinese) **25,** 935 (1996).
9. X. G. Zhang, N. Lin, T. Zhang, X. Liu, B. Yang, and L. Yu, Acta Photon. Sin. (in Chinese) **30,** 813 (2001).
10. D. Jia, B. Tan, Z. Wang, C. Ge, T. Yang, W. Ni, and S. Li, Chin. Opt. Lett. **4,** 318 (2006).
11. S. L. Liu and H. J. Zheng, Acta Opt. Sin. (in Chinese) **26,** 1313 (2006).
12. S. L. Liu and H. J. Zheng, Chinese J. Lasers (in Chinese) **33,** 199 (2006).